



# Modeling and simulation of the advanced structured surfaces machined by specially patterned grinding wheels via the structuring grinding process

Amr Monier<sup>1</sup> · Bing Guo<sup>1</sup> · Qingliang Zhao<sup>1</sup> · T. S. Mahmoud<sup>2</sup>

Received: 2 June 2021 / Accepted: 25 October 2021 / Published online: 6 January 2022  
© The Author(s), under exclusive licence to Springer-Verlag London Ltd., part of Springer Nature 2021

## Abstract

In this work, the ability to reshape the grinding wheels with patterns of special and modern geometries to produce the advanced structured surfaces is studied. Firstly, a mathematical model is built for the process relating the geometry of the grinding wheel, geometries of the wheel patterns, the produced structured surfaces, and the grinding operating parameters. Then, different regular and irregular geometries are designed to be patterned over the wheel surface. The regularly designed patterns include the circular, the elliptical, and the polygonal patterns, while the heart-like patterns are included as irregular ones. Afterward, a simulation method to express the patterned wheels and the corresponding structured surfaces at different working conditions is developed. The effects of the patterns' geometries on the obtained structured surfaces at the selected working conditions are investigated. The results of the grinding operations designed and carried out experimentally reflect the dependability of the presented method for machining the advanced structured surfaces using the grinding processes.

**Keywords** Grinding · Patterned grinding wheels · Structured surface · Modeling

## List of symbols

$n_x$	Number of pattern repetition per unit segment in $x$ direction	$\gamma_s$	Structuring ratio
$n_y$	Number of pattern repetition per unit segment in $y$ direction	$c_{xi}, c_{yi}$	Center coordinates of the pattern geometry in $x$ - $y$ plane
$A_t$	Total area of the wheel's unit segment	$x_i, y_i, z_i$	Coordinates of the point $p_i$ on the wheel's unit segment
$A_r$	Remained area of the wheel's unit segment	$p_{in}$	Points which are positioned inside the borders of patterns
$A_p$	Patterned area of the wheel's unit segment	$p_{out}$	Points which are positioned outside the borders of patterns
$a_s$	Area of single pattern of the unit segment	$r_c$	Radius of the designed patterns with circular geometry
		$r_{cs}$	Radius of the circumscribed circle for the designed patterns with polygonal geometry
		$L_{side}$	Side length of the designed patterns with polygonal geometry
		$N_{side}$	Sides number of the designed patterns with polygonal geometry
		$a, b$	Major and minor axes length of the designed patterns of elliptical geometry
		$d_s$	Depth of patterns
		$P_c$	Circular pitch
		$p_n$	The total number of points over each 2D wheel section
		$N$	Number of wheels' unit segments
		$R_g$	Wheel radius

✉ Bing Guo  
guobing@hit.edu.cn

✉ Qingliang Zhao  
zhaoqingliang@hit.edu.cn

Amr Monier  
amr.monier@hit.edu.cn

T. S. Mahmoud  
tamer.abdelmagid@feng.bu.edu.eg

<sup>1</sup> Center for Precision Engineering, School of Mechatronics Engineering, Harbin Institute of Technology, P.O. Box 413, Harbin, 150001, China

<sup>2</sup> Mechanical Engineering Department, Shoubra Faculty of Engineering, Benha University, Cairo, 11629, Egypt

$v_g$	Cutting velocity of the wheel
$v_w$	Feeding rate of the workpiece
$v^*$	Speed ratio
$d_c$	Grinding depth of cut
$\psi$	Helical angle between patterns' centers of the unit segment
$P$	Longitudinal pitch of surfaces structures
$S_w$	Width of a surface structure
$S_h$	height of a surface structure
$\vartheta$	Slope angle between centroids of workpiece's structures

## 1 Introduction

The increasing developments in the fields of modern industries and advanced manufacturing applications require producing surfaces with a determined function performance able to satisfy specific requirements. One frequent solution that has been recently applied is represented in the creation of the structured surfaces of parametric characteristics [1–3].

Through the use of the surfaces with structures, quantitative relationships can be established between the structural characteristics and the required functional performance of the surfaces. Surface structures should have characteristic parameters that can be designed according to both the selected manufacturing method and the demanded functions for engineering applications. In recent researches, it has been proved that surface structures improve effectively several areas in tribology such as friction, wear, lubrication, and energy consumption [4–6]. Hence, the research on manufacturing structures of controlled proprieties on the engineering surfaces is of great importance [7]. The significance of structured surfaces in modern applications can be found in several areas such as electronics [8], optics[9], and health [10].

Different methods can be used to fabricate the surface structures [11–13]. Recently, the grinding method has been used for machining surface structures in macro/micro-scale using what is called “structured grinding wheels” [14, 15]. This method is distinguished by its high efficiency, simplicity, and low cost. It produces various forms of surface structures repetitively without the need for additional manufacturing steps saving additional cost and time. Many studies have investigated the effect of using the structured/patterned grinding wheels on the overall process efficiency[16, 17]. To use the grinding process for machining a structured ground surface, the selected pattern should be formed on the wheel surface itself and subsequently transferred to the workpiece during processing operations. Modeling of the structuring grinding process to relate the properties of the final structure to the several operating parameters of the grinding method can be used for improving and optimizing the overall process efficiency.

Several studies used the grinding method to model and produce surface structures using the structured grinding wheel, but with some limitations on the obtained structured surfaces. Stpien [18, 19] used deep-dressed single/double-helical patterned wheels to produce the three basic shapes of structures on flat surfaces. Different processing conditions for successful surface structuring have been presented. Denkena et al. [20] used the profile grinding method to enhance the performance of turbine blades through fabricating structured riblets on their surfaces. This method showed the ability to machining the riblets under several grinding conditions resulted in reducing the friction and shear stresses and improving the blades' performance. Oliveira et al. [21, 22] presented other structuring methods that enabled forming preconfigured patterns on the wheels' surfaces by special dressing. Then, the patterns were moved out by grinding to the workpiece surfaces. Mohamed et al. [23] utilized the modeling method developed by Liu et al. [24] to predict the produced surface structures using the circumferentially structured grinding wheels. In the earlier work, Monier et al. [25] developed a new approach for machining the structured surfaces by grinding operations. Obtaining the designed surface structures under different grinding conditions has been explained.

The geometry of surface structures is one of the main characteristics that can be used for defining and controlling the properties of the structured surface. Machining surface structures in a repetitive way with different sizes controlled through the designed grinding parameters characterize the grinding method. However, the majority of the work found in the literature focused on the straight/helical patterns imprinted on the wheel surface and the related structures' geometries transferred to the workpiece surfaces. Studying the patternability of the grinding wheels with different advanced geometries and the related effects such as the geometrical shape, size, distribution, and degree of structuring on the obtained structured surfaces have not been studied before. This can enlarge the area of using the grinding method in machining the structured surfaces. Also, it can solve many limitations of the other applied methods either conventional or non-conventional to manufacture such structures' on the engineering surfaces. For instance, the stability, repeatability, and affected-zones of the laser texturing method on the engineering structured surfaces are influenced by several process parameters such as laser power and scan speed. This work aims to model and simulate patterning the grinding wheels with new and advanced pattern geometries and study their effects on the related structured surfaces.

Therefore, in this work, the ability for patterning the grinding wheel with advanced regular and irregular pattern geometries is presented. The effects of the designed wheel's patterns on the obtained structured surfaces at

different working conditions are investigated. A mathematical model for the process relating the wheel geometry, patterns' geometries, and the obtained structured surfaces at the designed operating parameters of the grinding process is built. Different regular and irregular patterns are defined and imprinted on the grinding wheels' surfaces. A simulation method using programming languages is examined for describing the structuring process and explaining the accompanied effects on the structured surfaces. Different parameters affecting the surface structuring process have been explained. The grinding experiments showed remarkable symmetries and a satisfied agreement between the simulated and the machined surfaces.

## 2 Modeling of grinding operations for the structured surfaces with special patterned grinding wheels

To create the model of the patterned grinding wheel, a unit segment is designed according to the pattern geometry required to be shaped on the wheel's surface. Figure 1 explains the principles for building the model of the patterned wheel's unit segment. In Fig. 1a, a 2D sketch for the designed unit segment with  $n_x$  by  $n_y$  number of patterns is shown. The geometrical pair ( $\Delta x$  and  $\Delta y$ ) represents the dimensions of the unit segment along the  $x$ -axis and  $y$ -axis respectively, while each wheel pattern has an area ( $a_s$ ). The proposed model assumes that the fraction of remained area ( $A_r$ ) of the unit segment is defined as "structuring ratio ( $\gamma_s$ )," such that:

$$\gamma_s = \frac{A_r}{A_t} \tag{1}$$

where ( $A_t$ ) is the total area of the unit segment. Then, the total patterned area ( $A_p$ ) of the unit segment can be determined as the following:

$$A_p = A_t \cdot (1 - \gamma_s) \tag{2}$$

Assuming a uniform area for all patterns, therefore:

$$a_s = \frac{A_p}{n_x \cdot n_y} \tag{3}$$

Then, the unit segment of the patterned wheel is converted to be a net and determined as an array of points in  $x$ - $y$  coordinates (see Fig. 1b). Assuming  $c_{xi}$  and  $c_{yi}$  are the center coordinates of the pattern area  $a_{si}$ , the model selects the optimum positions to place the patterns over the designed area of the unit segment. Afterward, the coordinates of all net's points either inside or outside the pattern area of the unit segment are identified by calculating mathematically the borders of each pattern area as follows:

$$f(x, y) = \begin{cases} f(x_i), & 1 \leq i \leq n \\ f(y_i), & 1 \leq i \leq n \end{cases} \tag{4}$$

where  $x_i$  and  $y_i$  are the coordinates of the  $i^{th}$  point of the unit segment.

Figure 2 shows different geometries designed to be patterned on the grinding wheel surface. If the designed patterns of the wheel have circular geometries, the borders can be mathematically determined by [26]:

$$(x_i - c_{xi})^2 + (y_i - c_{yi})^2 = r_c^2 \tag{5}$$

where  $r_c$  is the radius of the wheel circular pattern. For polygonal patterns, the side length  $L_{side}$  can be related to the circumscribed circle radius  $r_{cs}$  by:

$$L_{side} = 2 \cdot r_{cs} \cdot \sin\left(\frac{\pi}{N_{side}}\right) \tag{6}$$

where  $N_{side}$  represents the number of sides for the designed polygon.

For elliptical geometries:

$$\frac{x_i^2}{a^2} + \frac{y_i^2}{b^2} = 1 \tag{7}$$

where  $a$  and  $b$  are the major and minor axes half lengths of the elliptical pattern.

Moreover, irregular geometries such as heart-like shapes can also be modeled by controlling the driving formula

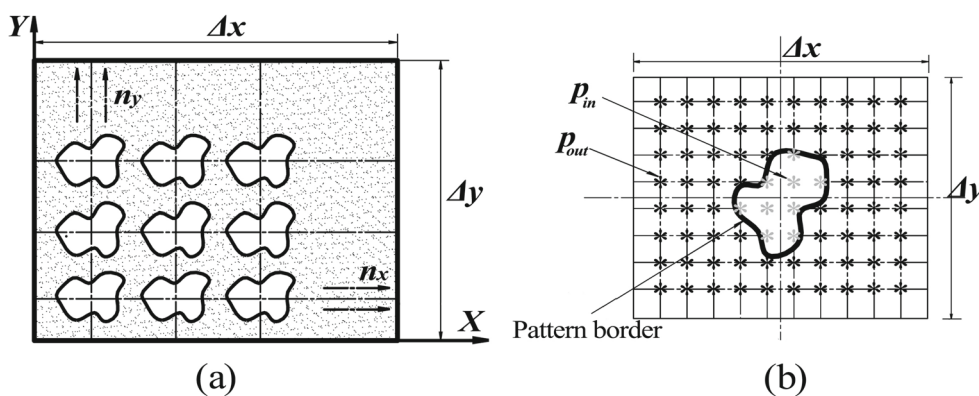
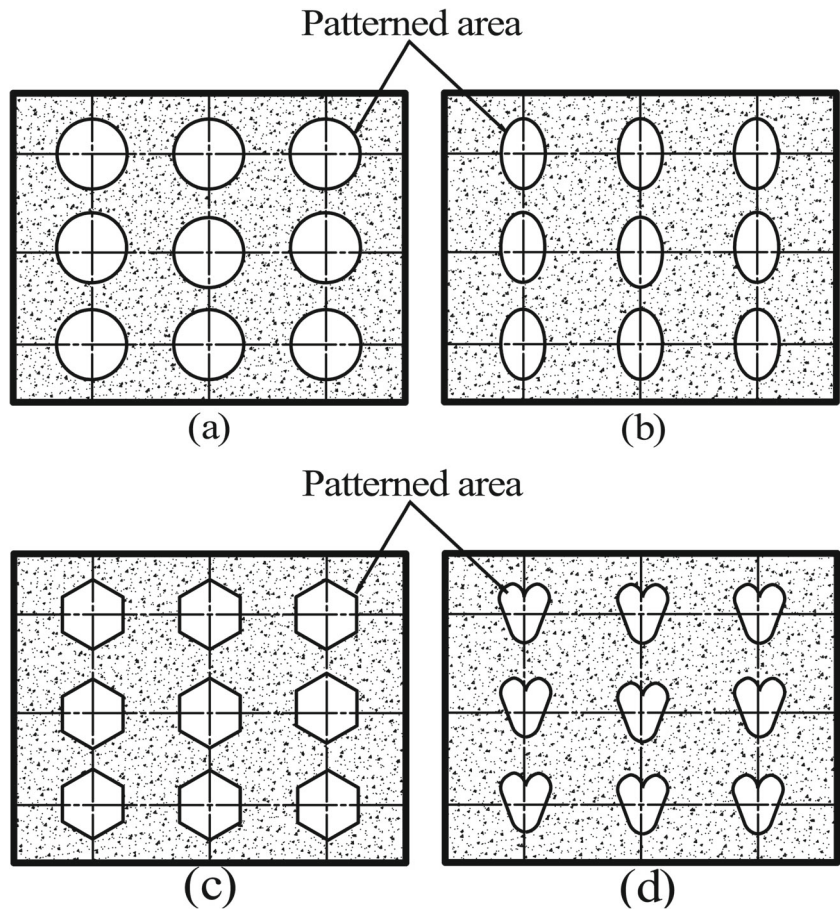


Fig. 1 (a) The designed unit segment of the grinding wheel in plain view, (b) defining of the point position over the unit segment

**Fig. 2** The different geometries for the wheel patterns, (a) the circular patterns, (b) the elliptical patterns, (c) the polygonal patterns, and (d) the heart-like patterns



for their  $x_i$  and  $y_i$  coordinates. For example, for heart-like geometries:

$$x_i = A \cdot \sin(\theta) \tag{8}$$

$$y_i = B \cos(\theta) + C \cos(2\theta) + D \cos(3\theta) + E \cos(\theta) + F \cos(14\theta) \tag{9}$$

where  $A, B, C, D, E,$  and  $F$  are constants.

After calculating the coordinates for all points of the unit segment in the  $x$ - $y$  plane, points' coordinates in  $z$ -direction represent their depths from the outer surface of the unit segment. The depth of a point  $p_i$  is specified according to its position over the unit segment area. If the designed patterns on the wheel surface have depth  $d_s$ , then  $z$  coordinates for the points inside patterns' borders are supposed to be of  $d_s$  values. Otherwise, the  $z$  coordinates become extinct. So, mathematically:

$$z_i = \begin{cases} 0 & p_i = p_{out} \\ d_s & p_i = p_{in} \end{cases} \tag{10}$$

where  $p_{in}$  and  $p_{out}$  represent the locations either inside or outside the pattern border respectively (see Fig. 1b).

After that, the points' coordinates in the  $x, y,$  and  $z$  directions are converted into the polar system and the unit

segment of the grinding wheel is created (see Fig. 3a). Then, the unit segment is repeated in the circumferential and radial directions to create the completed design of the patterned wheel shown in Fig. 3b. For simplicity, the unit segment is assumed to be repeated in one direction (circumferential direction). The circumferential distance from one point on a unit segment to the matching one on the next segment is titled “circular pitch  $P_c$ .” Assuming the grinding wheel has a radius ( $R_g$ ), the number of the unit segments that should

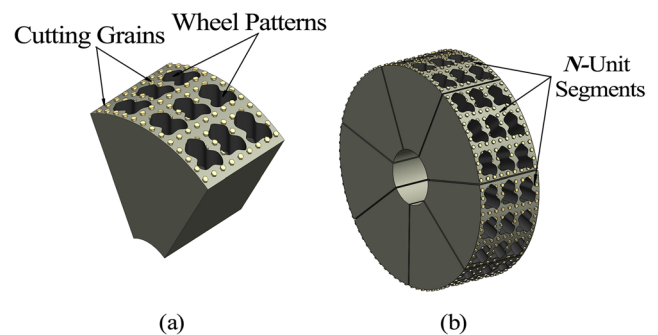


**Fig. 3** (a) The unit segment in polar coordinates and isometric view, (b) repeating the unit segment  $N$  times to build the grinding wheel



be repeated to create the complete shape of the patterned grinding wheel can be determined as:

$$N = \frac{2\pi \cdot R_g}{P_c} \tag{11}$$

Figure 4 illustrates the way followed to create the kinematic model for the patterned wheel. The wheel is divided into several sections cut across the wheel’s longitudinal axis. Each one is assumed to have a total number of points  $p_n$  represents the number of abrasive cutting grains. An abrasive point  $p_i$  is positioned at an angle  $(\alpha_i)$  and radius  $r(\alpha_i)$ . The polar position of the point ( $p_i$ ) is determined by the pair of parameters  $((\alpha_i)$  and  $r(\alpha_i)$ ) respectively. The angle  $(\varphi_i)$  determines the orientation of the point  $p_i$  from its home position after starting up the grinding operation. Using Eq. 10, the radial position of the point ( $p_i$ ) is calculated throughout subtracting the depth  $(d_s)$  from the wheel radius  $(R_g)$  and substituting in Eq.10 for  $z_i (p_i)$  by  $d_s(p_i)$ , therefore:

$$R_g = \begin{cases} R_g, & p_i = p_{out} \\ R_g - d_s, & p_i = p_{in} \end{cases} \tag{12}$$

After determining the polar position of all points around the wheel 2D section, all sections’ points are similarly specified and a complete definition of the wheel’s kinematic model is obtained.

Figure 5 explains the kinematics of the grinding operation proposed in this work to transfer the wheel patterns to the workpiece surface as structures. The grinding wheel and the workpiece operate at working velocities  $v_g$  and  $v_w$  respectively, while the grinding interaction between them is executed at  $(d_c)$  depth of cut. To get the structured surface, the presented model assumed that the grinding wheel rolls over the workpiece surface upon starting the grinding process as a result of the translation and the rotation motions in a perfect cycloidal path.

The structures over the workpiece surface are produced in such a way similar to that followed to build up the structured grinding wheel. The patterns shaped on each unit segment of the wheel surface are reflected on the workpiece

surface to a specific scale while the grinding wheel is rolling over the ground surface. As illustrated in Fig. 6, the linear distance on the workpiece surface between the engaging positions of two successive unit elements with the workpiece surface is named “longitudinal pitch  $P$ .” Accordingly, the circular pitch of the grinding wheel ( $P_c$ ) is related to the longitudinal pitch ( $P$ ) of the workpiece’s structures as follows:

$$P = P_c \cdot \frac{v_w}{v_g} = P_c \cdot v^* \tag{13}$$

And  $v^*$  is the ratio between the operating velocities of the workpiece and the grinding wheel respectively.

The geometry of each structure on the workpiece surface is defined by structure width ( $S_w$ ) and structure height ( $S_h$ ) (see Fig. 6). The structure width ( $S_w$ ) is the max-width of the workpiece surface structure in the direction parallel to the grinding direction. Similarly, the structure height ( $S_h$ ) is the max height of the structure over the workpiece ground surface. The values of the geometrical pair ( $S_w$  and  $S_h$ ) in addition to the longitudinal pitch ( $P$ ) are controlled by the grinding wheel geometry, the designed pattern geometry, and the operating parameters of the grinding process.

Figure 7 explains the effect of eccentricity between the patterns on the unit segment on the structured workpiece. In Fig. 7, the helical angle  $(\psi)$  defines the orientation of the distance between centers of wheel patterns from its longitudinal axis. The angle  $(\vartheta)$  represents the orientation of the centroids of the structures machined on the workpiece surface. According to the geometry shown in Fig. 7:

$$\tan \vartheta = \frac{P}{P_c} \cdot \tan \psi \tag{14}$$

Using Eq. 13, then:

$$\tan \vartheta = \frac{v_w}{v_g} \cdot \tan \psi \tag{15}$$

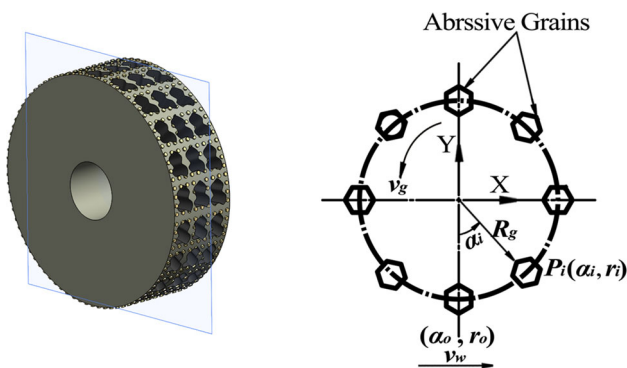


Fig. 4 The kinematic model of the patterned grinding wheel

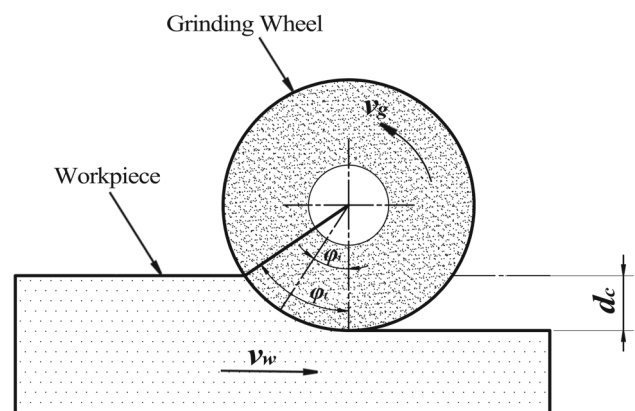
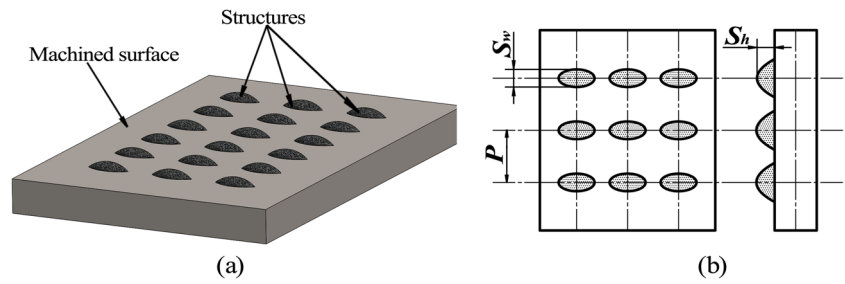


Fig. 5 A sketch of the kinematics of the grinding operation

**Fig. 6** (a) A sketch for the structured surface, (b) a plane view of the structured surface with its geometrical parameters



Then, in the case of up-grinding:

$$\vartheta = \arctan \left[ \frac{v_w}{v_g} \cdot \tan \psi \right] \tag{16}$$

In down-grinding:

$$\vartheta = \pi - \arctan \left[ \frac{v_w}{v_g} \cdot \tan \psi \right] \tag{17}$$

When the structuring grinding process starts up, the cycloidal path of any abrasive grain of the wheel and the scaled profile reflected on the workpiece surface can be supposed according to the time consumed during processing. The exhausted time  $t_i$  by the abrasive grain of number  $p_i$  to alternate its home position from  $(\alpha_i)$  to  $(\varphi_i)$  can be supposed as the following:

$$t_i = \frac{r_i}{v_g} \cdot (\varphi_i - \alpha_i) \tag{18}$$

Then, the path coordinates in the feeding direction ( $X_i$ ) and the direction normal to it ( $Y_i$ ) can be defined by:

$$\begin{cases} X_i(t) = v_w \cdot t_i + r_i \cdot \sin \varphi_i \\ Y_i(t) = R_g - d_g - r_i \cdot \cos \varphi_i \end{cases} \tag{19}$$

Using Eqs. 18 and 19, in the case of up-grinding:

$$\begin{cases} X_i(t) = v_w \cdot t_i + r_i \cdot \sin \left( \left( \frac{v_g}{r_i} \cdot t_i \right) + \alpha_i \right) \\ Y_i(t) = R_g - d_g - r_i \cdot \cos \left( \left( \frac{v_g}{r_i} \cdot t_i \right) + \alpha_i \right) \end{cases} \tag{20}$$

In down-grinding:

$$\begin{cases} X_i(t) = -v_w \cdot t_i + r_i \cdot \sin \left( \left( \frac{v_g}{r_i} \cdot t_i \right) + \alpha_i \right) \\ Y_i(t) = R_g - d_g - r_i \cdot \cos \left( \left( \frac{v_g}{r_i} \cdot t_i \right) + \alpha_i \right) \end{cases} \tag{21}$$

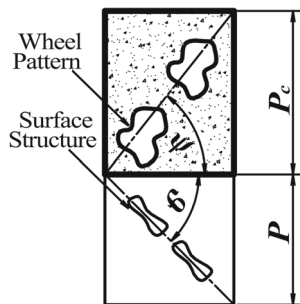


**Fig. 7** The relationship of the helical angle of wheel patterns with the slope angle of surface structures

### 3 Simulation results and discussion

Simulation of the structuring grinding processes using programming languages is an attractive way for estimating both the designed patterned wheels and the obtained structured surfaces at different operating parameters. This can serve in optimizing the structuring process and selecting the proper parameters to get the aimed characteristics of structures. Also, it facilitates understanding and explaining the changing behavior of the structured surfaces under several working conditions. The simulation process depends on the geometry of the grinding wheel, the geometry of the wheel pattern, and the working parameters of the grinding operation. The geometry of the grinding wheel is defined by the wheel radius ( $R_g$ ) and the structuring ratio ( $\gamma_s$ ). The geometry of the wheel pattern will be defined later in the following sections. The grinding parameters includes the working velocities ( $v_g$  and  $v_w$ ) and the grinding depth of cut ( $d_c$ ). In this study, the wheel geometry and the grinding parameters are designed to be constant while the major changes happen to the pattern's geometrical parameter. This is aiming to clarify the effects of the patterns' geometrical parameters on the ground surface structures with being affected neither by the wheel geometry nor the grinding parameters.

On the other side, the geometry of the structured surfaces resulted from wheels with different patterns and at determined grinding conditions will be simulated and evaluated. The geometry of the structures produced on the workpiece surface is determined by the values of the structure width ( $S_w$ ), the structure height ( $S_h$ ), the longitudinal pitch ( $P$ ), and the slope angle ( $\vartheta$ ). The ability of the presented model to estimate the structured surfaces produced by the designed wheels of regular and irregular patterns mentioned in the previous section will be measured. This is illustrated in the subsequent sections.

#### 3.1 Simulation of the structured surfaces produced by patterned wheels of round patterns

The first design presented for the patterned grinding wheels is the round patterns. This includes wheels with circular patterns and elliptical patterns. For the circular patterns, the

pattern geometry is defined by the radius of the circular pattern ( $r_c$ ). For the elliptical patterns, half lengths of the major and minor axes ( $a$  and  $b$ ) control the pattern geometry. Also, the pattern geometry includes the required helical angle ( $\psi$ ) and the depth of the patterns ( $d_s$ ) produced on the wheel surface. Table 1 includes the geometrical parameters of the grinding wheel and the selected grinding condition used to study the circular pattern. Table 2 contains different designs for the circular patterns required to be shaped on the grinding wheel surface.

Figure 8 shows the unit segments of the circular patterns mentioned in Table 2, the grinding wheels, and the related structured surfaces with 2D profiles across the unit lengths of structures. As shown in Fig. 8, when the radius ( $r_c$ ) of the wheel pattern increases while the structuring ratio ( $\gamma_s$ ) is constant, the number of patterns per unit segment on the wheel surface decreases. Additionally, the designed value of the unit segment area ( $A_t$ ) increases. Redesigning of both parameters is performed taking into consideration that the fraction of the remained area of the unit segment to be constant. Hence, the structuring ratio ( $\gamma_s$ ) keeps its value equal to the designed one listed in Table 1 (see Eq. 1). So, the peripheral distance between the successive patterns increases. In this figure, the difference in the number of patterns, the pattern depths, and the helical angle between centers can be noted.

For the side of the structured surfaces, it can be shown that as the pattern radius ( $r_c$ ) increases, the structure width ( $S_w$ ), the structure height ( $S_h$ ), and the longitudinal pitches ( $P$ ) between surface structures increase (see Fig. 8 and Table 3). The reason is that, by increasing the pattern radius ( $r_c$ ), the circumferential distance between wheel patterns increases and the number of patterns over the wheel surface decreases. If the circumferential distance between centers of two successive patterns is considered as the circular pitch ( $P_c$ ) of the patterned wheel. Therefore, the circular pitch ( $P_c$ ) of the patterned wheel and the related longitudinal pitch ( $P$ ) on the workpiece surface increase with the increasing pattern radius ( $r_c$ ). Hence, the structure width ( $S_w$ ) increases with the increasing longitudinal pitch ( $P$ ) allowing the structure's height ( $S_h$ ) to acquire a higher value.

Moreover, assuming the number of the workpiece's surface structures per unit length is defined as "structures linear density (structures  $LD$ ).” Therefore, the structures  $LD$  decreases with the increasing pattern radius ( $r_c$ ). This can be explained as the rate of the passing patterns over

the workpiece surface decrease, for the same grinding condition, with the increasing pattern radius ( $r_c$ ). The change in structures  $LD$  with the increasing pattern radius can be shown clearly in Fig. 8 (a, b, c) where the 2D profiles are taken across the unit length of surface structures. To increase the structures  $LD$  at a raising value of the pattern radius ( $r_c$ ), the velocity ratio should be modified.

The previous explanation is agreed with the modeling principles explained and formulated in Section 2. Table 3 includes the geometrical parameters for the structured surfaces illustrated in Fig. 8.

The structuring ratio ( $\gamma_s$ ) of patterned wheels can also control the degree of surface structuring. Figure 9 shows different designs for the circular patterned wheel mentioned in Table 2 with number (b) and the related structured surfaces but at an increasing value for the structuring ratio ( $\gamma_s$ ) and a zero helical angle ( $\psi = 0$ ). The increasing structuring ratio is achieved by raising the area of the unit segment and keeping the patterns' geometrical parameters as designed. This increases the fraction of remained area of the unit segment and the structuring ratio ( $\gamma_s$ ) as well (see Eqs. 2 and 11).

Comparing the unit segments, patterned wheels, and structured surfaces in Fig. 9 with that shown in Fig. 8b. It is clear that as the structuring ratio ( $\gamma_s$ ) increases, the total number of patterns on the wheel surface decreases. As the increasing structuring ratio requires decreasing the fraction of patterned area of the grinding wheel (see Eq. 1). Therefore, the circular pitch ( $P_c$ ) and the related longitudinal pitch ( $P$ ) increase, while the structures  $LD$  decreases with the increasing structuring ratio ( $\gamma_s$ ) (see Fig. 9). However, the structure width ( $S_w$ ) and the structure height ( $S_h$ ) of the workpiece surface structures have not changed from that shown in Fig. 8b as the patterns geometry and the operating parameters are similar.

For the elliptical patterns, the selected operating parameters for the wheel geometry and the grinding process are found in Table 4. The designed geometries for the elliptical patterns are declared in Table 5. Figure 10 illustrates the elliptical patterned wheels and the related structured surfaces obtained using the working condition stated in Table 4. Similarly, the increasing pattern size at the constant structuring ratio ( $\gamma_s$ ) is compensated by decreasing the number of patterns per unit segment on the wheel surface and increasing the unit segment area ( $A_t$ ) (see Fig. 10). As a result, the longitudinal pitch ( $P$ ) and the size ( $S_w$  and  $S_h$ )

**Table 1** The proposed parameters for the wheel geometry and the grinding process with the circular patterned wheels

Wheel radius ( $R_g$ ) mm	Structuring ratio ( $\gamma_s$ )	Depth of cut $d_c$	Velocity ratio $v^*$
15	0.5	0.01	0.10

**Table 2** The designed geometrical parameters for the circular patterns of the grinding wheel

Circular pattern No.								
a			b			c		
$r_c$ (mm)	$d_s$ (mm)	$\psi$ (deg)	$r_c$ (mm)	$d_s$ (mm)	$\psi$ (deg)	$r_c$ (mm)	$d_s$ (mm)	$\psi$ (deg)
0.5	0.5	0	0.65	0.65	30	0.80	0.8	45

of workpiece surface structures increase, but the structures  $LD$  decreases with the increasing pattern size. Table 6 contains the geometrical parameters of the structured surfaces represented in Fig. 10.

Also, in Fig. 11, an example for the elliptical patterned wheel of number (b) in Table 5 (at zero helical angle ( $\psi$ )) and the related structured surfaces at an increasing structuring ratio ( $\gamma_s$ ) is figured out. The behavior of the structured surfaces with the increasing structuring ratio ( $\gamma_s$ ) is similar

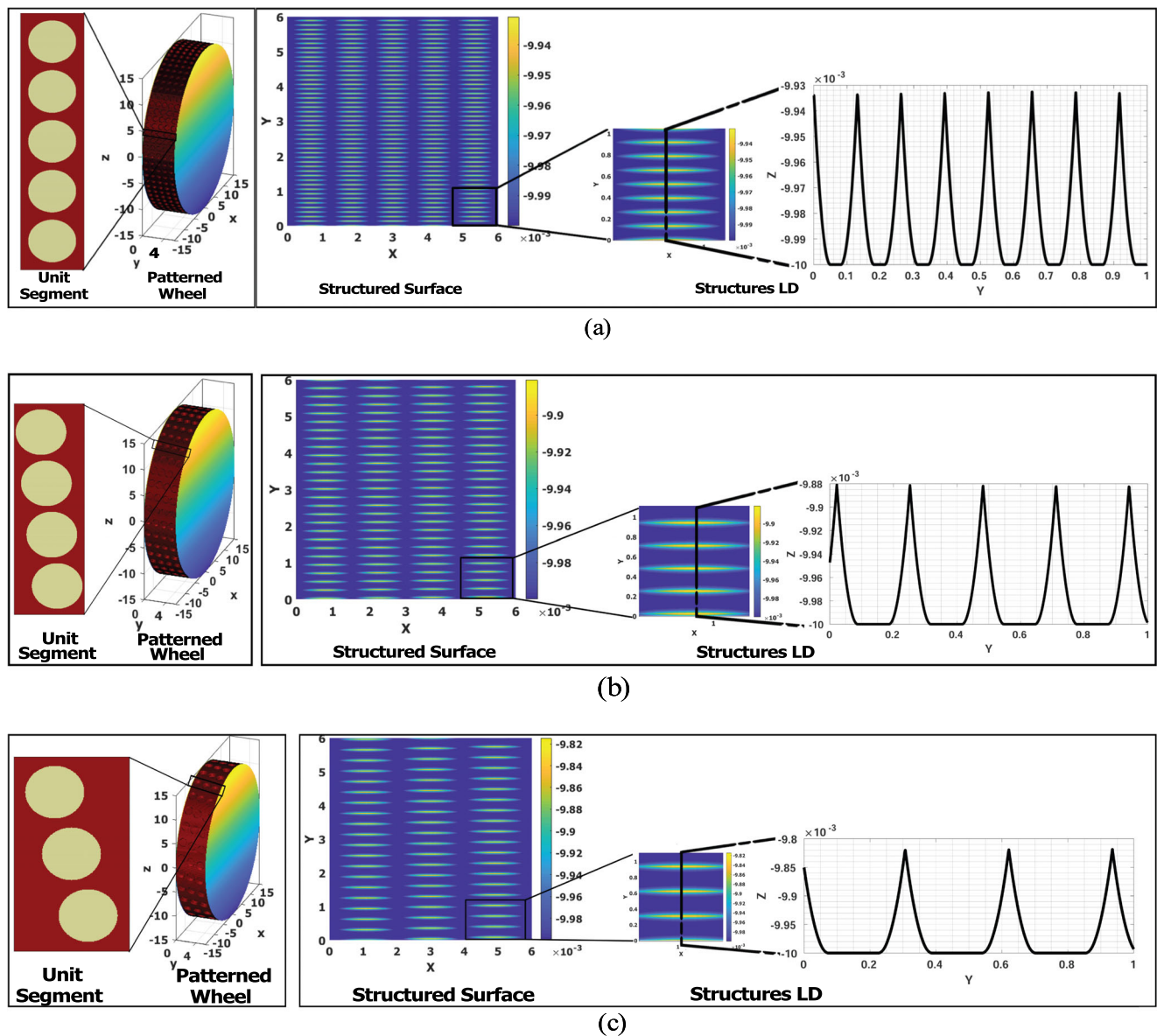


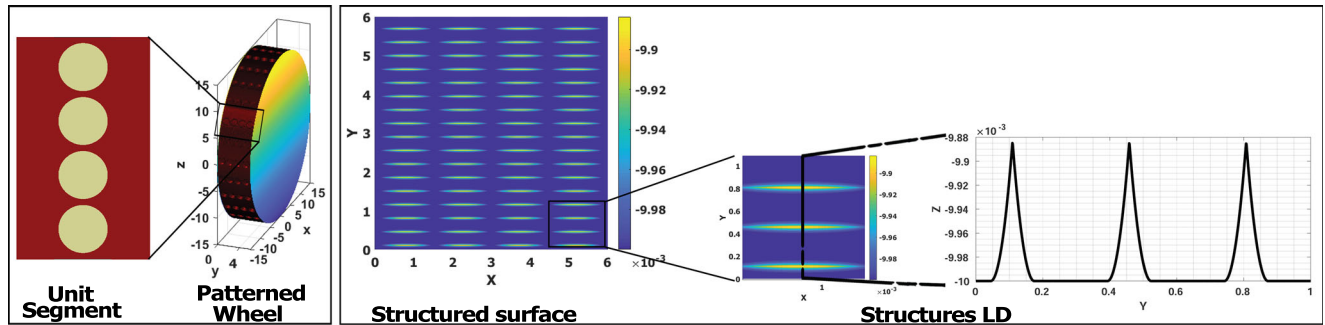
**Fig. 8** The grinding wheels and the related structured surfaces with different geometries of the circular patterns



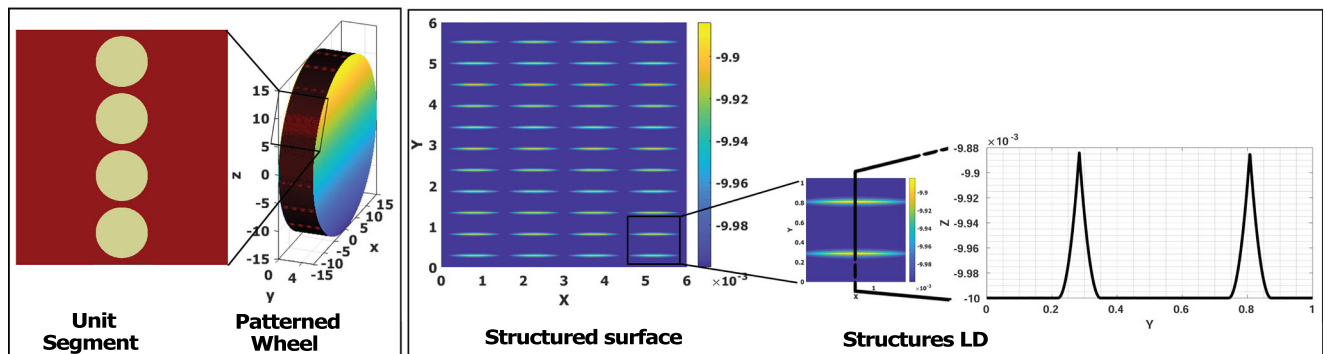
**Table 3** The geometrical parameters of the structured surfaces obtained by the circular patterned wheels

The structured surface of circular pattern *No.*

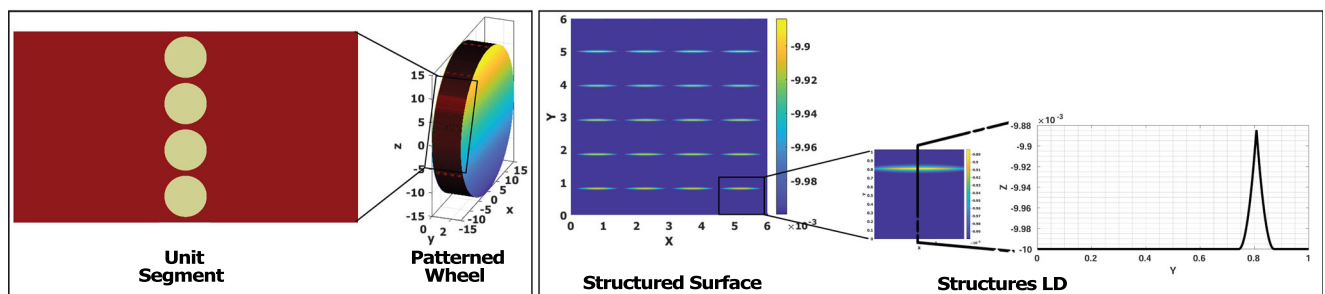
a				b				c			
$S_w$ (mm)	$P$ (mm)	$\vartheta$ (deg)	$S_h$ ( $\mu\text{m}$ )	$S_w$ (mm)	$P$ (mm)	$\vartheta$ (deg)	$S_h$ ( $\mu\text{m}$ )	$S_w$ (mm)	$P$ (mm)	$\vartheta$ (deg)	$S_h$ ( $\mu\text{m}$ )
0.085	0.131	0	0.070	0.112	0.234	3.31	0.120	0.129	0.300	5.71	0.182



(a)



(b)



(c)

**Fig. 9** The circular patterned wheels and the related structured surfaces at the increasing structuring ratio: (a)  $\gamma_s = 0.75$ , (b)  $\gamma_s = 0.83$ , and (c)  $\gamma_s = 0.91$

**Table 4** The proposed parameters for the wheel geometry and the grinding process with the elliptical patterned wheels

Wheel radius ( $R_g$ ) mm	Structuring ratio ( $\gamma_s$ )	Depth of cut $d_c$	Velocity ratio $v^*$
20	0.73	0.01	0.128

**Table 5** The designed geometrical parameters for the elliptical patterns of the grinding wheel

Elliptical pattern No.

a				b				c			
$a$ (mm)	$b$ (mm)	$d_s$ (mm)	$\psi$ (deg)	$a$ (mm)	$b$ (mm)	$d_s$ (mm)	$\psi$ (deg)	$a$ (mm)	$b$ (mm)	$d_s$ (mm)	$\psi$ (deg)
0.50	0.25	0.5	0	0.65	0.325	0.65	30	0.80	0.40	0.8	45

to that of the circular patterned wheels. The geometry of the structure itself is the same for all patterned wheels similar

to that shown in Fig. 10b. But, the longitudinal pitches ( $P$ ) between structures increase and structures  $LD$  decreases

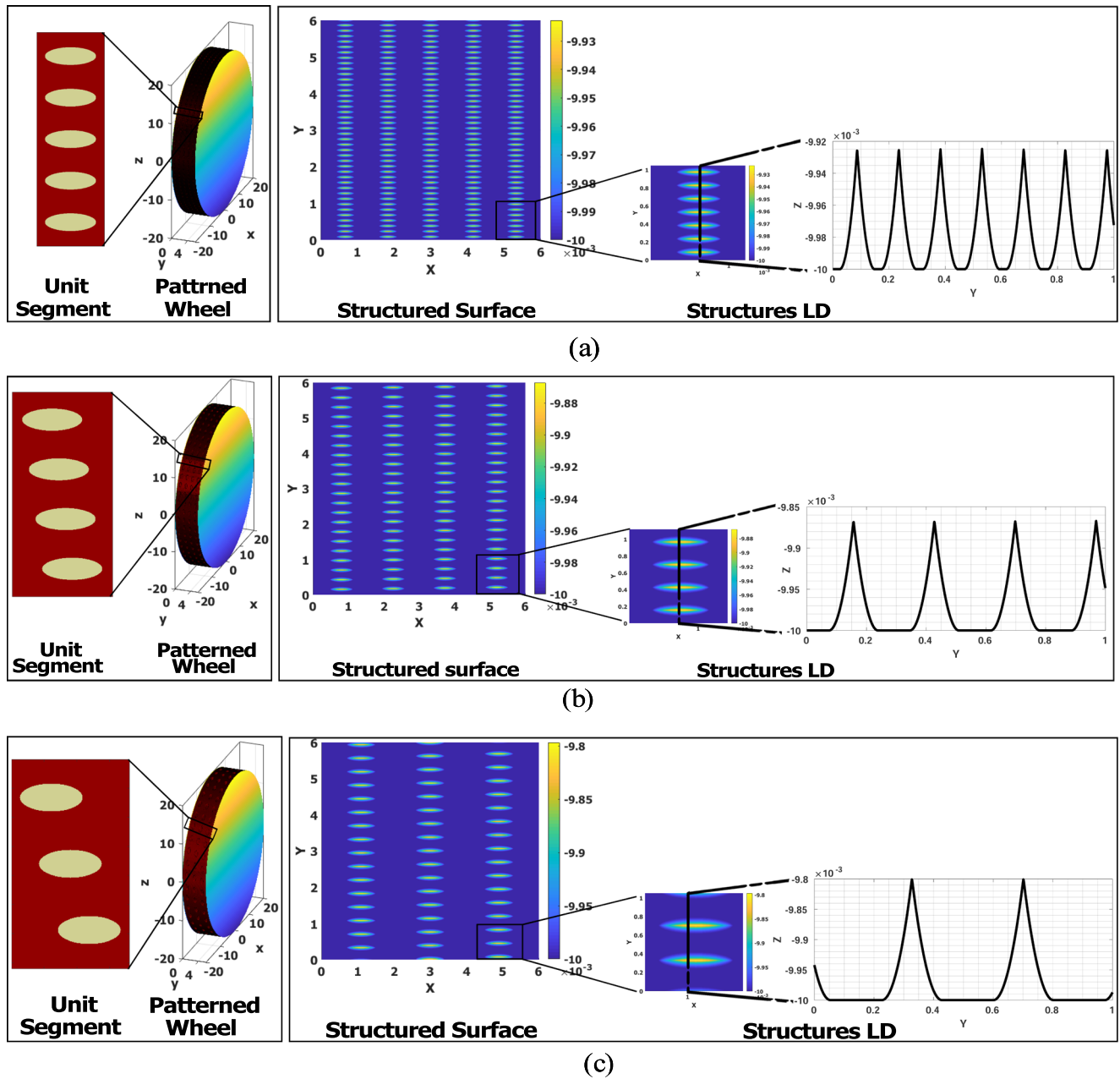


**Fig. 10** The grinding wheels and the related structured surfaces with different geometries for the elliptical patterns

**Table 6** The geometrical parameters of the structured surfaces obtained by the elliptical patterned wheels

The structured surface of elliptical pattern *No.*

a				b				c			
$S_w$ (mm)	$P$ (mm)	$\vartheta$ (deg)	$S_h$ ( $\mu\text{m}$ )	$S_w$ (mm)	$P$ (mm)	$\vartheta$ (deg)	$S_h$ ( $\mu\text{m}$ )	$S_w$ (mm)	$P$ (mm)	$\vartheta$ (deg)	$S_h$ ( $\mu\text{m}$ )
0.097	0.152	0	0.0758	0.133	0.274	4.23	0.130	0.174	0.387	7.30	0.200

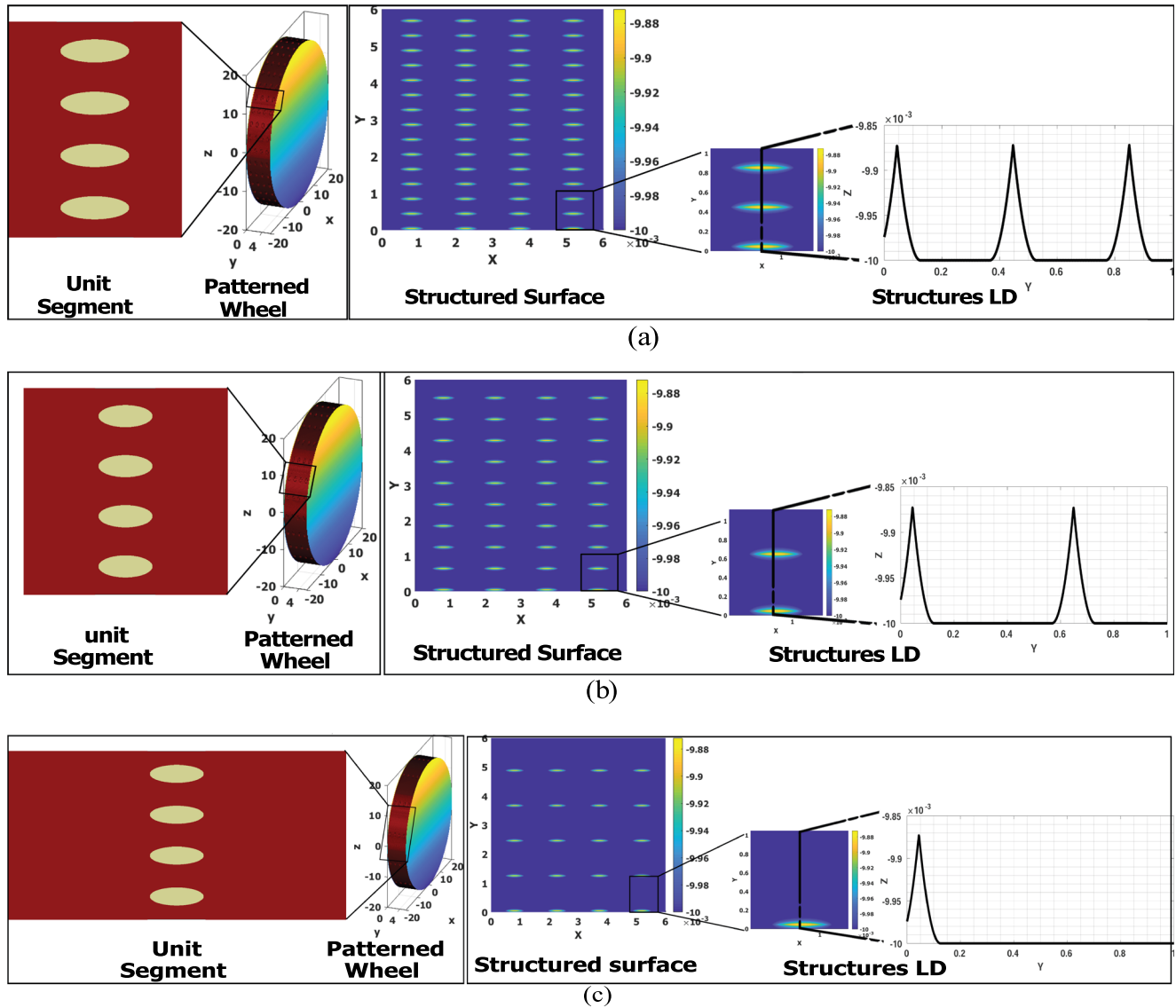


**Fig. 11** The elliptical patterned wheels and the related structured surfaces at the increasing structuring ratio: (a)  $\gamma_s = 0.86$ , (b)  $\gamma_s = 0.90$ , and (c)  $\gamma_s = 0.95$

**Table 7** The proposed parameters for the wheel geometry and the grinding process with the polygonal patterned wheels

Wheel radius ( $R_g$ ) mm	Structuring ratio ( $\gamma_s$ )	Depth of cut $d_c$	Velocity ratio $v^*$
15	0.65	0.01	0.167

**Table 8** The designed geometrical parameters for the polygonal patterns of the grinding wheel

Polygonal pattern No.

a				b				c			
$r_c$ (mm)	$N_{side}$	$d_s$ (mm)	$\psi$ (deg)	$r_c$ (mm)	$N_{side}$	$d_s$ (mm)	$\psi$ (deg)	$r_c$ (mm)	$N_{side}$	$d_s$ (mm)	$\psi$ (deg)
0.50	4	0.5	0	0.65	6	0.65	30	0.80	8	0.8	45

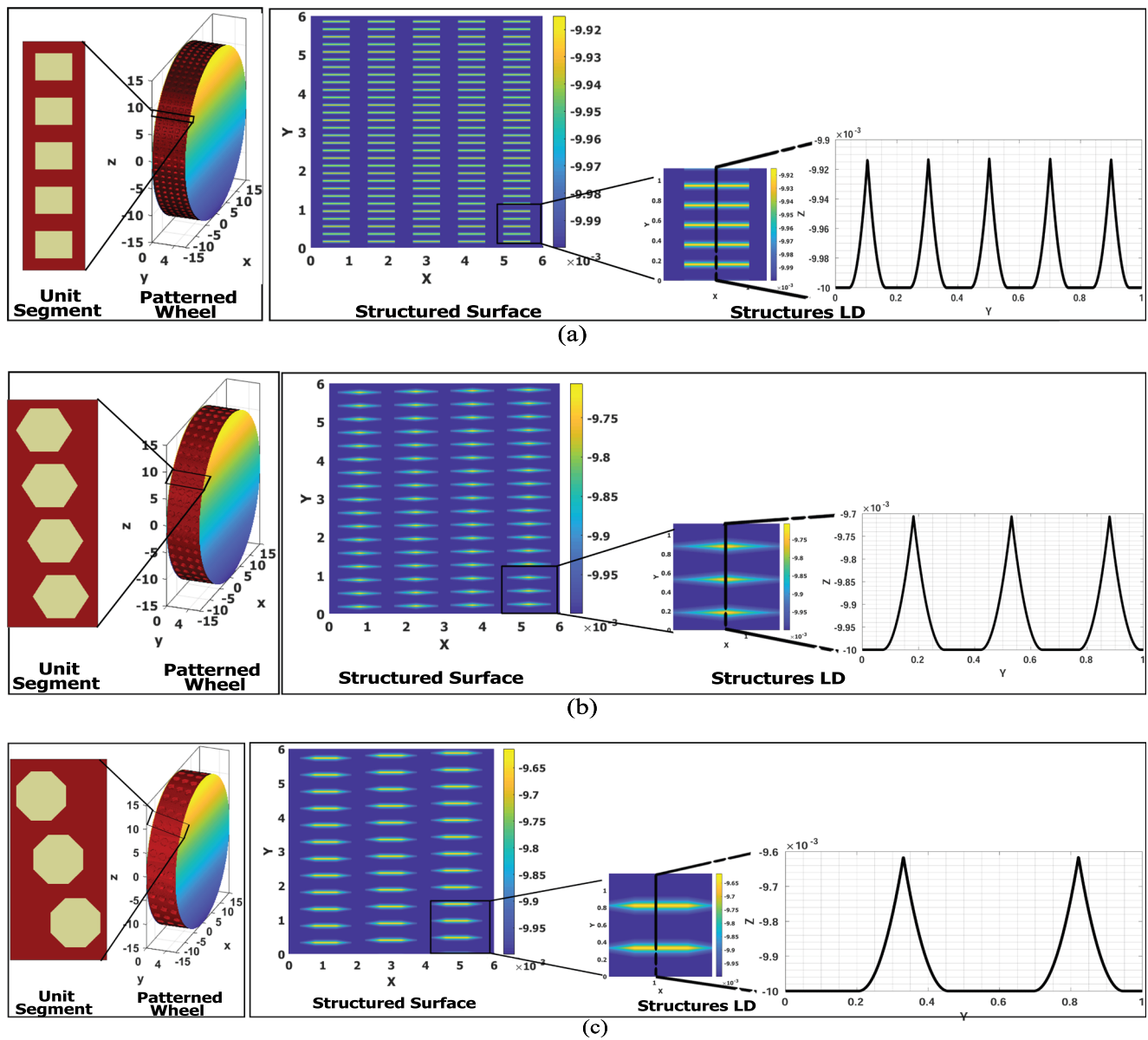


**Fig. 12** The grinding wheels and the related structured surfaces with different polygonal patterns



**Table 9** The geometrical parameters of the structured surfaces obtained by the polygonal patterned wheels

The structured surface of polygonal pattern *No.*

a				b				c			
$S_w$ (mm)	$P$ (mm)	$\vartheta$ (deg)	$S_h$ ( $\mu\text{m}$ )	$S_w$ (mm)	$P$ (mm)	$\vartheta$ (deg)	$S_h$ ( $\mu\text{m}$ )	$S_w$ (mm)	$P$ (mm)	$\vartheta$ (deg)	$S_h$ ( $\mu\text{m}$ )
0.167	0.199	0	0.850	0.217	0.349	5.50	0.294	0.248	0.491	9.46	0.745

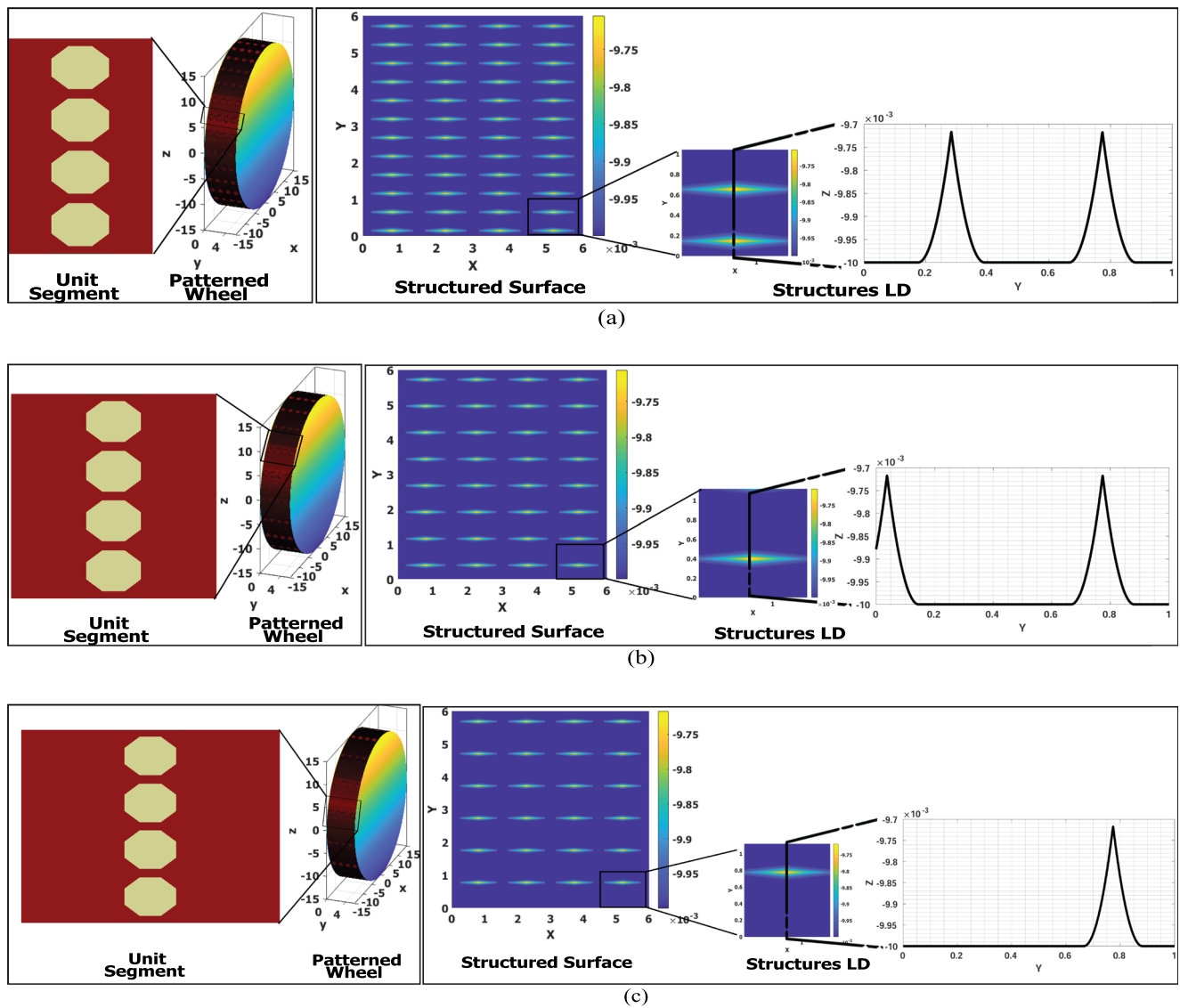


**Fig. 13** The polygonal patterned wheels and the related structured surfaces at the increasing structuring ratio: (a)  $\gamma_s = 0.73$ , (b)  $\gamma_s = 0.84$ , and (c)  $\gamma_s = 0.89$

due to the increasing circular pitch ( $P_c$ ) accompanied to the increasing structuring ratio ( $\gamma_s$ ).

### 3.2 Simulation of the structured surfaces produced by patterned wheels of polygonal patterns

Next, the structured surfaces produced by grinding wheels of polygonal patterns are investigated. In this study, the geometry of the polygonal pattern is defined by the circumscribed circle radius ( $r_{cs}$ ) and the number of the polygon's sides ( $N_{side}$ ). The operating conditions used in this investigation for the geometry of the grinding wheel and the grinding process are listed in Table 7.

Table 8 includes the geometries of the polygonal patterns designed to be formed on the grinding wheel surface. Three types of polygonal patterns have been tried with different geometrical parameters. This includes square, hexagonal, and octagonal patterns at increasing values of the circumscribed circle radius ( $r_{cs}$ ), number of sides ( $N_{side}$ ), and the helical angle ( $\psi$ ).

Figure 12 shows the unit segments of the polygonal patterns mentioned in Table 8, the grinding wheels, and the related structured surfaces with 2D profiles across the structures  $LD$ . The differences in the size and the type between the designed patterned wheels are obvious in Fig. 12. With the increasing size of the polygonal pattern

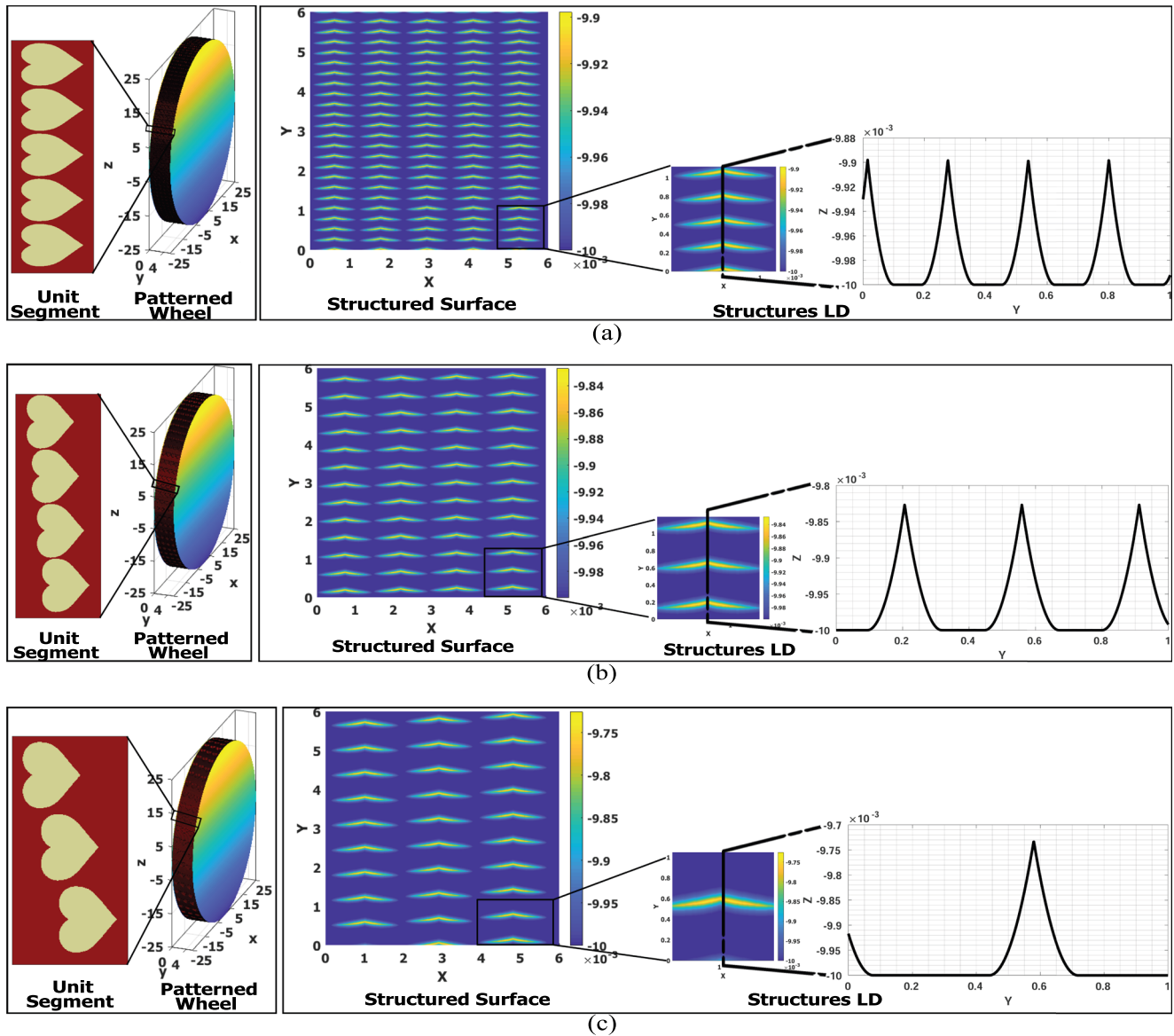


Fig. 14 The grinding wheels and the related structured surfaces at different heart-like pattern sizes

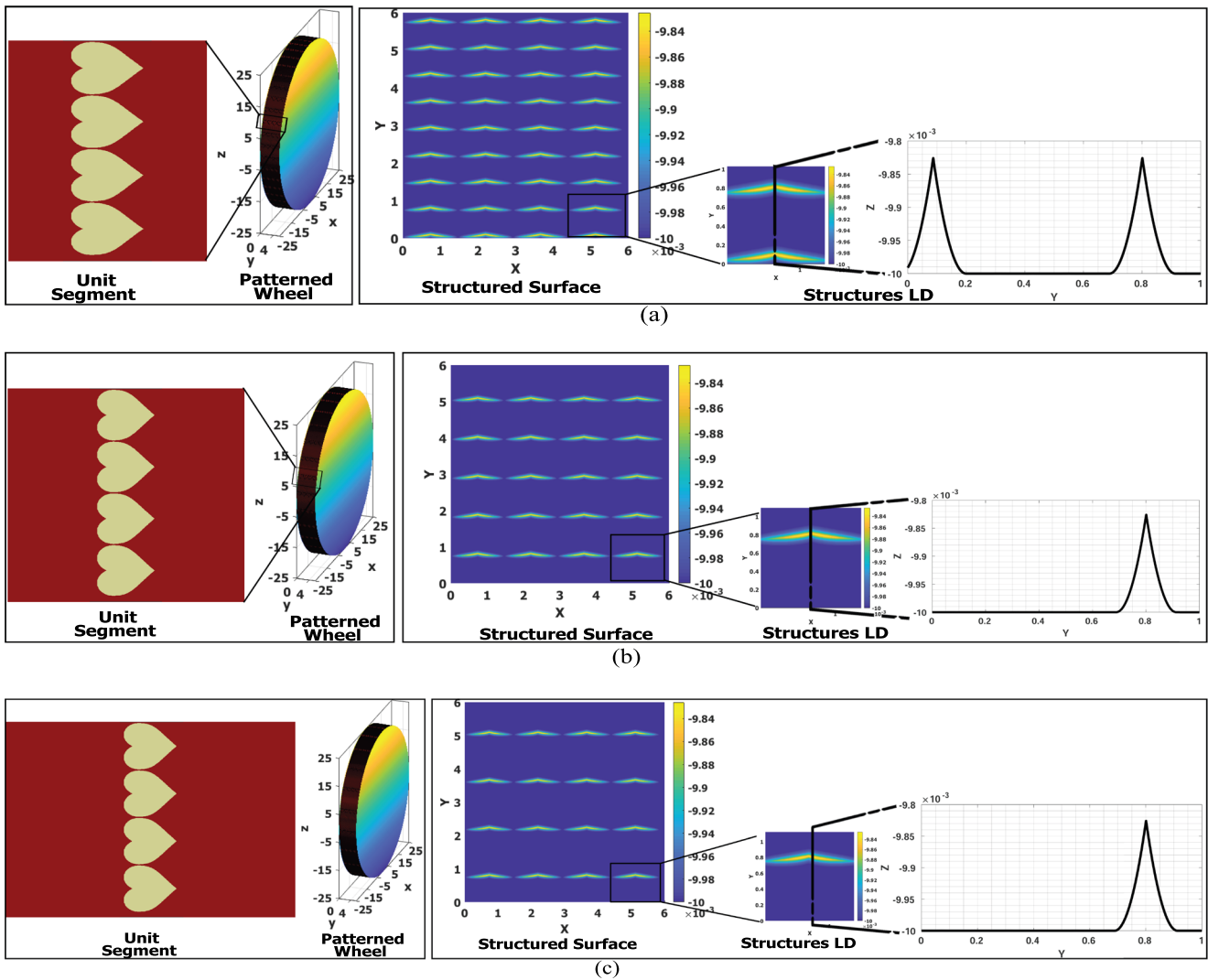


Fig. 15 The heart-like patterned wheels and the related structured surfaces at the increasing structuring ratio

at fixed structuring ratio ( $\gamma_s$ ), the number of patterns on the wheel surface and the structures  $LD$  of the workpiece surface decreases and the area of unit segment increases.

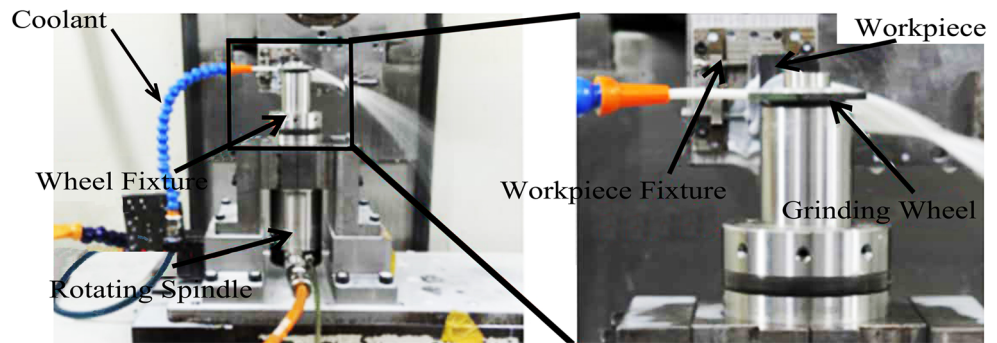
The geometry of the surface structure and the values of its geometrical parameters are affected by the pattern type

and the pattern size of the grinding wheel. It can be noted on the surface structures and their enlarged views that the workpiece structures are reflections of the wheel patterns on the workpiece surface. The dimensions of wheel's patterns that are parallel to the grinding direction are scaled on



Fig. 16 The ultra-precision surface grinder

**Fig. 17** (a) Components of the ultra-precision surface grinder, (b) mounting of the grooved wheel and the workpiece specimens in position



the workpiece surface. But, the others which are normal to the grinding direction keep the same designed values of the patterns on the wheel surface. Table 9 includes the geometrical parameters of the structured surfaces shown in Fig. 12.

On the other side, the same procedures followed with the round patterns to illustrate the effect of the changing structuring ratio ( $\gamma_s$ ) on the structured surface are tracked with the polygonal ones. Figure 13 displays the patterned wheels of hexagonal patterns designed in Table 6 but at increasing value of the structuring ratio ( $\gamma_s$ ). The influence of the structuring ratio ( $\gamma_s$ ) of the wheel on the obtained structured surfaces is clear. The geometry of the structures on the workpiece surfaces shown in Fig. 13 is the same as that shown in Fig. 12b but at larger values of the longitudinal pitch ( $P$ ). This refers to the increasing circular pitch ( $P_c$ ) of the wheel patterns with the increasing structuring ratio ( $\gamma_s$ ) (see Eq. 13). The similarity in behavior of the structured surfaces at the analogous working conditions with the different types of wheel patterns proves the efficiency of the presented model for representing the structured surfaces machined with the specially designed patterned wheels.

### 3.3 Simulation of the structured surfaces produced by patterned wheels of irregular patterns

In addition to the regular geometries, grinding wheels with irregular patterned geometries and the corresponding surface structures are going to be investigated. Unlike regular patterns, controlling the geometries of irregular patterns is to some extent more complex than regular ones. It can be done by changing and controlling several parameters of the driving formulas (see Eqs. 8–9). In this study, the heart-like pattern is presented as an example for the irregular geometry of patterned wheels. The obtained surface structures at increasing values for the pattern size and the helical angle ( $\psi$ ) are being analyzed.

Figure 14 demonstrates the heart-like patterned wheels and the corresponding structured surfaces obtained at an enlarging pattern size and the same grinding parameters. In this figure, it can be observed that as the pattern size increases, the number of patterns on the wheel surface decreases and the circular pitch ( $P_c$ ) between them increases. This intends to minimize the changes in the structuring ratio ( $\gamma_s$ ) of the heart-like patterned wheel while the pattern size is increasing as explained before with regular patterned ones.

**Fig. 18** The model and the real view of the grooved wheel used for carrying out experimental work ( $N = 2$ ,  $\gamma_s = 0.50$ ,  $\psi = 0$  deg)

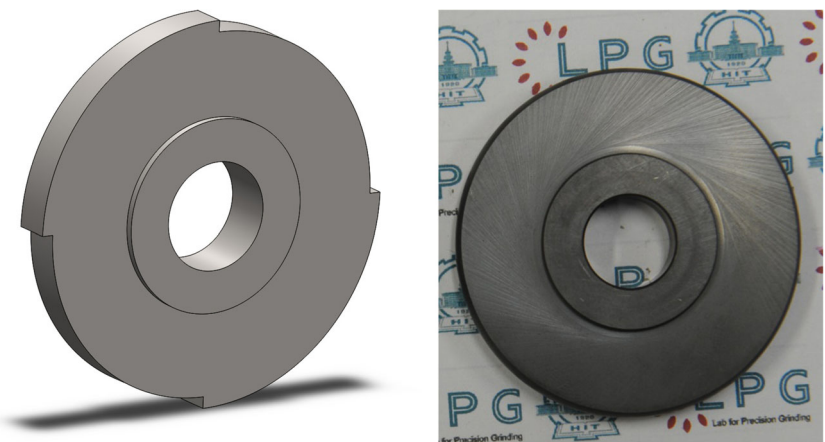




**Table 10** Working conditions at the changing velocity ratio

Experiment No.	Wheel velocity <i>RPM</i>	Feed rate (mm/min)	Velocity ratio $v^*$	Depth of cut $d_c$ (mm)
a	500	800	0.0102	0.002
b	600	700	0.0074	0.002
c	700	700	0.0064	0.002
d	500	676	0.0086	0.002

Also, different from the regular geometries, the irregularity of pattern geometry at the increasing size may allow the pattern to exceed the unit segment borders. So, the designed dimensions of the unit segments ( $\Delta x$  and  $\Delta y$ ) should be modified to accommodate the increasing value of the pattern size within the unit segment borders.

Furthermore, regarding the structured surfaces, the structures' behavior accompanied to the increasing size of the heart-like pattern is to a high extent analogous to those regular. As the pattern size increases, the structure width ( $S_w$ ), the structure height ( $S_h$ ), and the longitudinal pitch ( $P$ ) of surface structures increase as well. By contrast, the structures  $LD$  decreases with the increasing size of the wheel pattern. In addition, the pattern dimensions parallel to the grinding direction are scaled on the workpiece's structured surface. While the others normal to the grinding direction keep the same values as the designed wheel pattern (see Fig. 14).

Besides, Fig. 15 displays the patterned wheels and the structured surfaces of the heart-like pattern at an increasing structuring ratio ( $\gamma_s$ ). The raised structuring ratio ( $\gamma_s$ ) is realized by growing up the unit segment area while the designed pattern retains the same size. In this figure, as the structuring ratio ( $\gamma_s$ ) increases, the degree of surface structuring decreases. This refers to the rising longitudinal pitch ( $P$ ) between structures and the falling structures  $LD$  due to the increasing circular pitch ( $P_c$ ) (see Eq. 13). However, the size of structures ( $S_w$  and  $S_h$ ) has not been affected because of the constant geometry of the pattern size operating at a similar working condition.

The matching attitudes of the results between regular and irregular patterned wheels at changing working conditions and the consistency with the mathematical model can be considered an evidence for the efficiency of the presented method for designing, predicting, and manufacturing the structured surfaces with the specially designed regular and/or irregular patterned wheels.

**Table 11** Working conditions at the changing depth of cut

Experiment No.	Wheel velocity <i>RPM</i>	Feed rate (mm/min)	Velocity ratio $v^*$	Depth of cut $d_c$ (mm)
a	500	900	0.0115	0.002
b	500	900	0.0115	0.003
c	500	900	0.0115	0.004
d	500	900	0.0115	0.006

### 4 Verification and experimental work

In this section, the ability and the accuracy of the presented model to predict and produce the structured surfaces are going to be measured and evaluated. As shown in Fig. 16, MUGK7120X5 ultra-precision surface grinder has been constructed to be used as the experimental platform. A KAISER electric spindle was installed on the moving table of the surface grinder and adapted to move along the  $X$ -axis direction of the surface grinder. A laser displacement sensor was used for setting the axis eccentricity. The dynamic balance of the spindle was detected throughout balancing screws, and the spindle was adjusted to run under balanced working conditions.

The balance deviation was set to be not more than 1 nm to ensure stable operating conditions at high speeds and to meet the requirements of precision grinding operations. Afterwards, the patterned wheel was mounted on the electric spindle using a special designed fixture, and the wheel runout has been minimized. Then, tungsten carbide (WC) workpiece specimens have been mounted in position for performing the structuring processes on the machined surfaces (see Fig. 17).

Figure 18 illustrates the geometry of the grinding wheel used in the current experimental work. A super abrasive diamond grinding wheel of 25 mm radius was prepared by pulsed laser machining system and a motorized translation stage was used for setting the grinding wheel in position to perform the laser structuring process. The grinding wheel is structured by a ratio of 50% in two straight grooves to be used in performing the structuring processes.

In this work, two sets of grinding experiments have been designed. In the first set, the velocity ratio ( $v^*$ ) was varying by changing the values of working velocities while the grinding depth of cut ( $d_c$ ) was constant. For the other one, the depth of cut ( $d_c$ ) was changing and



Fig. 19 The white light interferometer

the velocity ratio ( $v^*$ ) was kept fixed. Here, the selected parameters for the velocity ratio and the depth of cut ( $v^*$  and  $d_c$ ) are assigned according to the designed geometry of machined microstructures and the performance of the grinding machine tool. This aims to machine the surface structures successfully and ensure the accuracy of predicted results under several working conditions at the state of stability. Tables 10 and 11 include the designed values of the working parameters selected for both sets of experiments respectively. Then, a white light interferometer (WLI) was used for inspection and analysis of the structured surfaces' morphologies after executing the grinding operations. The device is illustrated in Fig. 19.

The longitudinal pitch ( $P$ ) and structure width ( $S_w$ ) have been selected for the evaluation and comparison between the predicted and ground geometries of the obtained surface structures. Figure 20 includes the values for both parameters at the designed experiments' sets. Figure 20a represents the results for experiments carried out at varying velocity ratio ( $v^*$ ) (Table 10), while Fig. 20b involves the results for those proceeded at changing depth of cut ( $d_c$ ) (Table 11). The simulated results are represented by the contentious lines

while the single points are the experimental values produced at the same operating parameters.

Figure 21 displays the simulated and the machined structured surfaces obtained at the working conditions listed in Table 10. The behavior of the longitudinal pitch with the changing velocity ratio is as expected. While the velocity ratio ( $v^*$ ) is decreasing (Fig. 21 (a)–(c)), the pitch ( $P$ ) values decrease. When the velocity ratio ( $v^*$ ) increases (Fig. 21 (d)), the pitch ( $P$ ) starts rising. Table 12 contains the values of the geometrical parameters for the simulated and the machined surfaces shown in Fig. 21. Figure 22 shows the obtained structured surfaces using the working conditions listed in Table 11 at the changing grinding depth ( $d_c$ ). Table 13 contains the values of the obtained geometries at the second set of the grinding conditions. Here, as the velocity ratio ( $v^*$ ) is constant, the pitch ( $P$ ) values for the simulated and ground surfaces are approximately constant as well. A satisfied agreement can be noted between the simulated and the machined values for the geometrical parameters of the structured surfaces for both experiments sets.

Additionally, in Figs. 21 and 22, differences in morphologies between the structured parts and the ground parts over each machined surfaces are obvious. This refers to the different formation mechanisms of both parts of the machined surface. During the grinding process, remained parts of the wheel surface are responsible for forming the ground parts of the workpiece surface, while the edges of the wheel's patterns reshape the workpiece's structures. The different number of active abrasive grains and the related cut chips between the two regions of the wheel result in the divergence between parts of the workpiece surface. Usually, the structured parts are rougher than the ground parts over the workpiece surface.

Also, there are variations between the machined surfaces at varying velocity ratio and those proceeded at changing

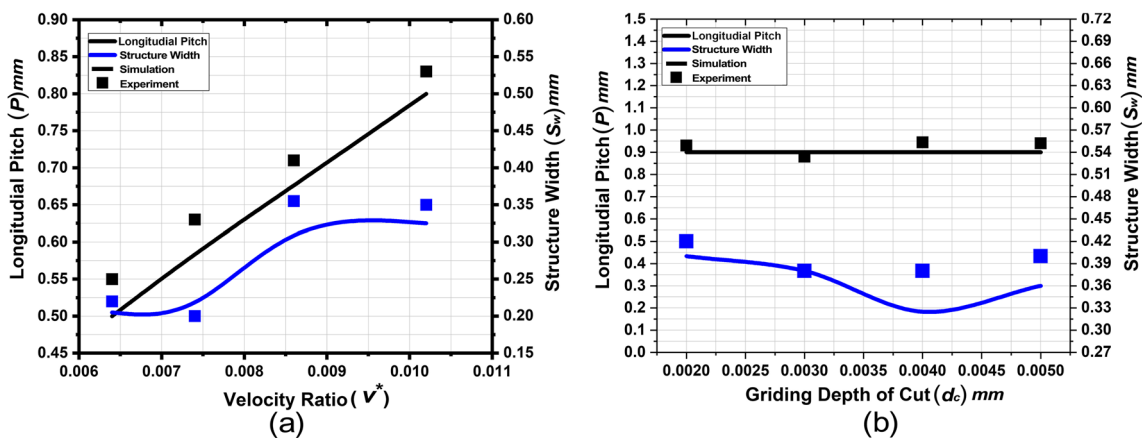


Fig. 20 The values of simulated and experimental geometrical parameters for the machined surface structures at the designed grinding experiments

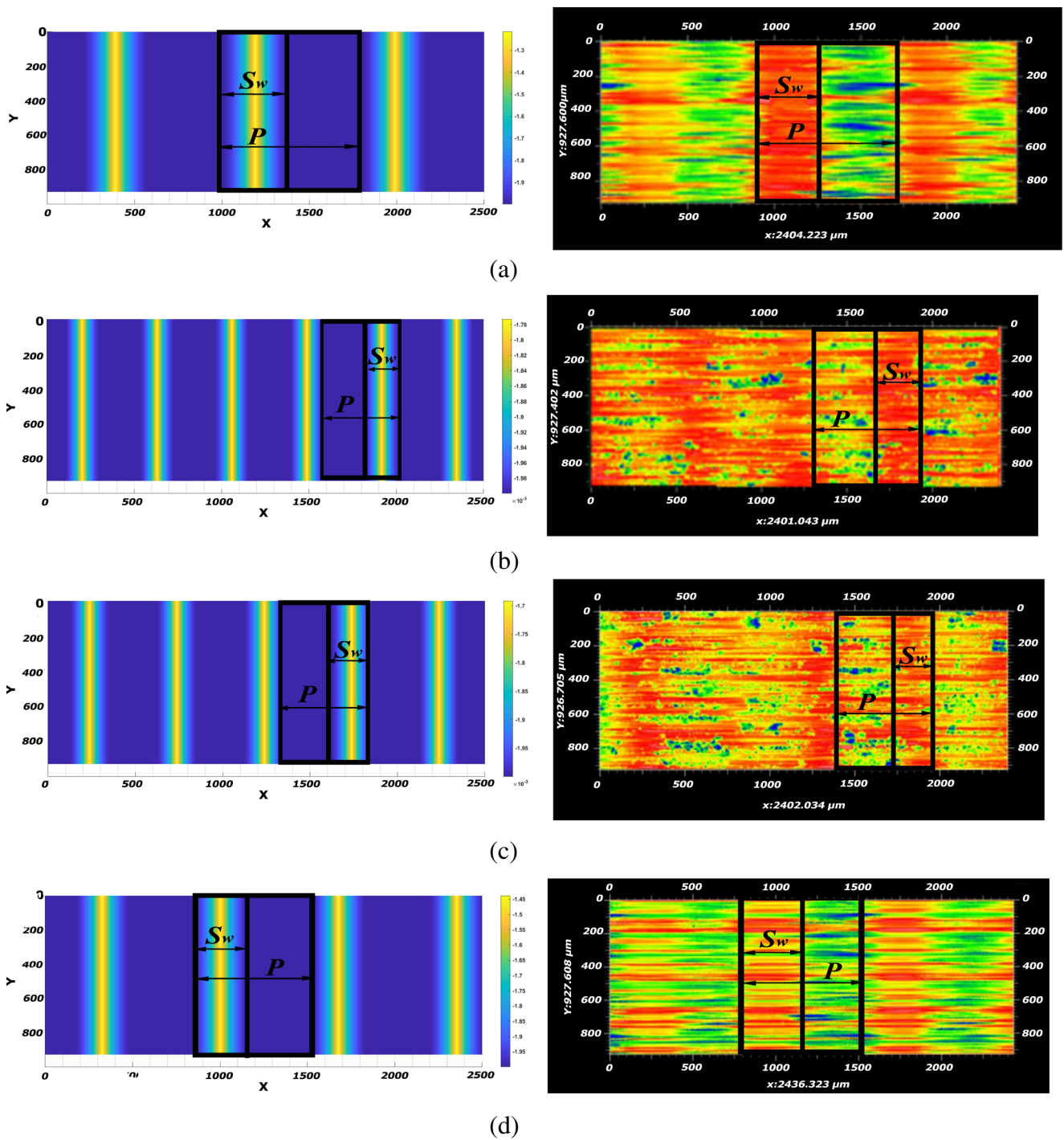


Fig. 21 The simulated and the experimental structured surfaces at the changing velocity ratio (dimensions in  $\mu\text{m}$ )

**Table 12** Values of the obtained simulated and machined geometrical parameters of the structured surfaces at different velocity ratios

No.	Structure width ( $S_w$ ) mm		Longitudinal pitch ( $P$ ) mm	
	Simulation	Machining	Simulation	Machining
a	0.325	0.350	0.800	0.830
b	0.195	0.200	0.590	0.630
c	0.205	0.220	0.500	0.540
d	0.338	0.355	0.680	0.710

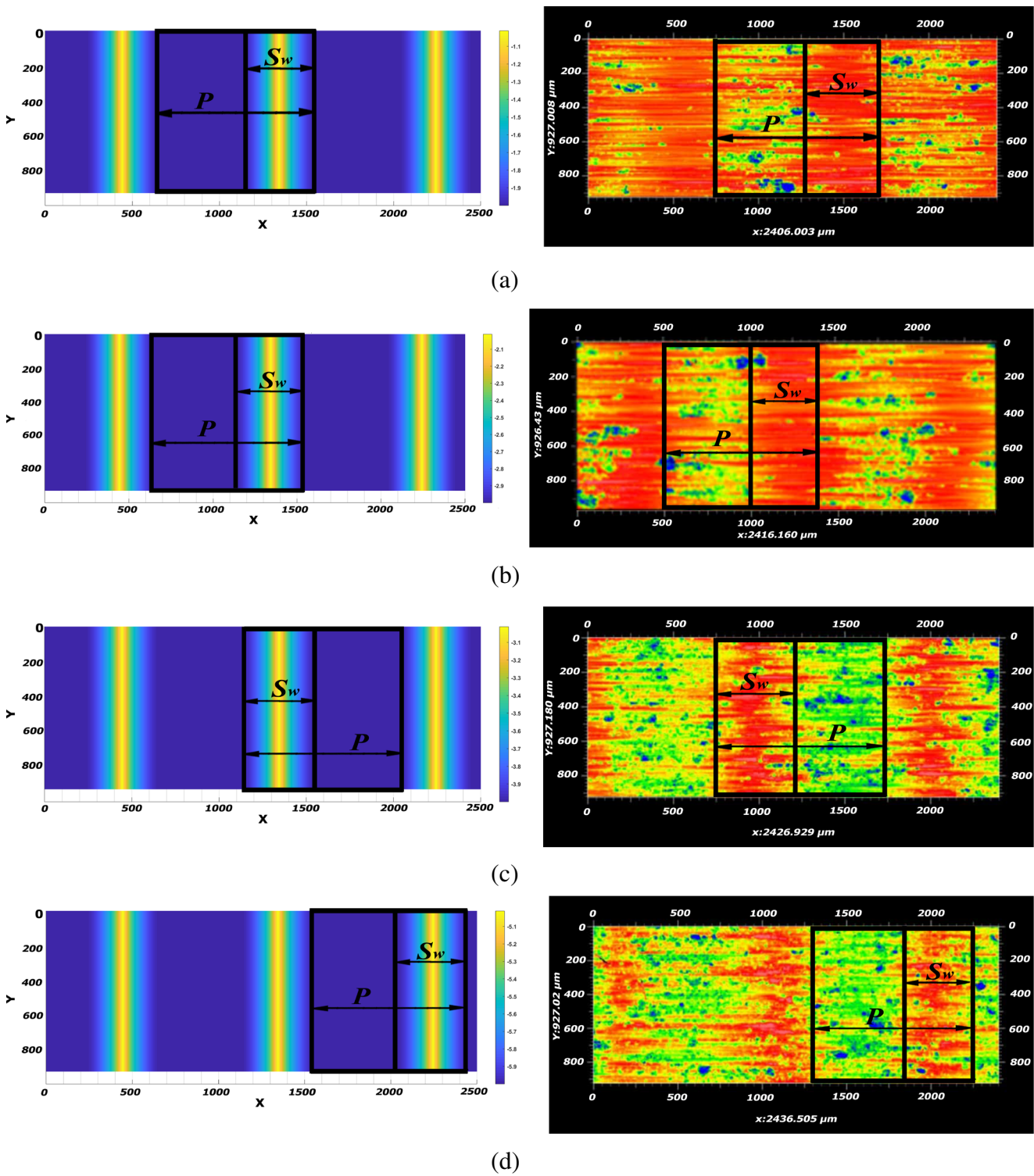


Fig. 22 The simulated and the machined surfaces at varying grinding depth (dimensions in  $\mu\text{m}$ )



**Table 13** The simulated and the machined surfaces at varying grinding depth (dimensions in  $\mu\text{m}$ )

No.	Structure width ( $S_w$ ) mm		Longitudinal pitch ( $P$ ) mm	
	Simulation	Machining	Simulation	Machining
a	0.400	0.420	0.900	0.930
b	0.380	0.380	0.900	0.880
c	0.325	0.380	0.900	0.940
d	0.360	0.400	0.900	0.940

cutting depth. These variations are due to the different influences of both parameters at the nanoscale grinding operation. According to Li et al. [27, 28], at increasing grinding velocity, the machined surface becomes smoother because of the higher chipping volume and the reduced surface damage. On the other side, the higher depth of cut raises the energy consumption and surface damage which reduce the efficiency of the grinding operation.

## 5 Conclusion

In this paper, the ability for machining the structured surfaces using specially designed patterned wheels has been studied. This tends to widen the applicability of the grinding method in designing and manufacturing advanced structured surfaces. A mathematical model is built for the process, and a simulation method is developed. Several regular and irregular patterns have been applied. The influences of the wheel patterns on the structured surfaces have been demonstrated and verified throughout running the grinding experiments. The conclusions are as follows:

1. Machining of the structured surfaces by the grinding method using special designed geometries for the wheel patterns is applicable. Different regular and irregular patterns such as circular, elliptical, polygonal, and heart shapes at different working conditions are formulated and simulated.
2. At increasing pattern size and constant structuring ratio, the number of patterns on the wheel surface decreases, and the circumferential distances separating them on the wheel surface increase.
3. As the size of wheel patterns grows up, the size of workpiece structures increase and structures linear density decreases. The structure width, the structure height, and the longitudinal pitches between structures increase.
4. At constant wheel pattern size, the structuring ratio of grinding wheels controls the structures linear density by adjusting the longitudinal pitch between structures without affecting the size of the surface structure itself.
5. Dimensions of the wheel patterns parallel to the grinding direction are scaled on the workpiece surface

unlike those normal to the grinding direction which don't differ from those ones designed on the wheel.

### Author contribution

**Amr Monier:** conceptualization, methodology, investigation, software, validation, data curation, supervision, formal analysis, writing—original draft, writing—reviewing and editing.

**Bing Guo:** methodology, software, resources, supervision, funding acquisition, project administration, validation, resources, reviewing—original draft.

**Qingliang Zhao:** resources, supervision, funding acquisition, project administration, validation visualization, measurements, formal analysis, reviewing—original draft.

**T.S.Mahmoud:** formal analysis, investigation, data curation, validation, reviewing—original draft.

**Funding** This work was supported by the National Natural Scientific Foundation of China (Grant No.: 51405108) and Enterprise Innovation and Development Joint Program of the National Natural Science Foundation of China (Grant No.: U20B2032).

**Availability of data and materials** The manuscript has not been published previously (partly or in full) elsewhere.

### Declarations

**Ethics approval** All procedures performed in studies involving human participants were in accordance with the ethical standards of the institutional and/or national research committee and with the 1964 Helsinki declaration and its later amendments or comparable ethical standards. This article does not contain any studies with human participants or animals performed by any of the authors.

**Consent to participate** Informed consent was obtained from all individual participants included in the study.

**Consent for publication** Informed consent was obtained from all individual participants included in the study.

**Competing interests** The authors declare no known competing interests.

### References

1. Bruzzone AAG, Costa HL, Lonardo PM, Lucca DA (2008) Advances in engineered surfaces for functional performance. CIRP annals 57(2):750–769

2. De Chiffre L, Kunzmann H, Peggs GN, Lucca DA (2003) Surfaces in precision engineering, microengineering and nanotechnology. *CIRP Annals* 52(2):561–577
3. Galda L, Pawlus P, Sep J (2009) Dimples shape and distribution effect on characteristics of stribeck curve. *Tribol Int* 42(10):1505–1512
4. Ibatan T, Uddin MS, Chowdhury MAK (2015) Recent development on surface texturing in enhancing tribological performance of bearing sliders. *Surf Coat Technol* 272:102–120
5. Costa HL, Hutchings IM (2007) Hydrodynamic lubrication of textured steel surfaces under reciprocating sliding conditions. *Tribol Int* 40(8):1227–1238
6. Costa HL, Hutchings IM (2009) Effects of die surface patterning on lubrication in strip drawing. *J Mater Process Technol* 209(3):1175–1180
7. Denkena B, Boehnke D, Spille C, Dragon R (2008) In-process information storage on surfaces by turning operations. *CIRP annals* 57(1):85–88
8. Wang F, Zhang X, Wang L, Jiang Y, Wei C, Zhao Y (2015) Pyramidal texturing of silicon surface via inorganic–organic hybrid alkaline liquor for heterojunction solar cells. *J Power Sources* 293:698–705
9. Cho C, Kim H, Jeong S, Baek S-W, Seo J-W, Han D, Kim K, Park Y, Yoo S, Lee J-Y (2013) Random and v-groove texturing for efficient light trapping in organic photovoltaic cells. *Solar Energy Materials and Solar Cells* 115:36–41
10. Zhang J, Meng Y (2012) A study of surface texturing of carbon steel by photochemical machining. *J Mater Process Technol* 212(10):2133–2140
11. Li HN, Yue Y, Zhao YJ, Zhang Z, Zhu W, Wang W, Qi H (2019) On the periodicity of fixed-abrasive planetary lapping based on a generic model. *J Manuf Process* 44:271–287
12. Zhang F, Meng B, Geng Y, Zhang Y (2016) Study on the machined depth when nanoscratching on 6h-sic using berkovich indenter: Modelling and experimental study. *Appl Surf Sci* 368:449–455
13. Guo B, Zhao Q, Yu X (2014) Surface micro-structuring of coarse-grained diamond wheels by nanosecond pulsed laser for improving grinding performance. *Int J Precision Eng Manuf* 15(10):2025–2030
14. Li HN, Axinte D (2016) Textured grinding wheels: a review. *Int J Mach Tools Manuf* 109:8–35
15. Forbrigger C, Bauer R, Warkentin A (2017) A review of state-of-the-art vitrified bond grinding wheel grooving processes. *Int J Adv Manuf Technol* 90(5):2207–2216
16. Zhang X, Kang ZX, Li S, Wu QP, Zhang Z (2018) Experimental investigations on the impact of different laser macro-structured diamond grinding wheels on alumina ceramic. *Int J Adv Manuf Technol* 96(5):1959–1969
17. Deng H, He J (2017) A study of the grinding performance of laser micro-structured coarse-grained diamond grinding wheels. *Int J Adv Manuf Technol* 93(5):1989–1997
18. Stpień P, Szafarczyk M (1989) Generation of regular patterns on ground surfaces. *CIRP annals* 38(1):561–566
19. Stpień P (2009) Regular surface texture generated by special grinding process. *J Manuf Sci Eng*, 131(1)
20. Denkena B, Köhler J, Wang B (2010) Manufacturing of functional riblet structures by profile grinding. *CIRP J Manuf Sci Technol* 3(1):14–26
21. da Silva EJ, Gomes de Oliveira JF, Salles BB, Cardoso RS, Alves Reis VR (2013) Strategies for production of parts textured by grinding using patterned wheels. *CIRP Annals* 62(1):355–358
22. Oliveira JFG, Bottene AC, Franca TV (2010) A novel dressing technique for texturing of ground surfaces. *CIRP annals* 59(1):361–364
23. Mohamed AL-MO, Warkentin A, Bauer R (2017) Prediction of workpiece surface texture using circumferentially grooved grinding wheels. *Int J Adv Manuf Technol* 89(1-4):1149–1160
24. Liu Y, Warkentin A, Bauer R, Gong Y (2013) Investigation of different grain shapes and dressing to predict surface roughness in grinding using kinematic simulations. *Precision Engineering* 37(3):758–764
25. Monier A, Guo B, Zhao Q, Liu W (2021) Strategy and error analysis for machining the designed microstructured surfaces by structured grinding wheels. *Int J Adv Manuf Technol* 113(5):1361–1376
26. Meserve BE (2014) *Fundamental concepts of geometry*. Courier Corporation
27. Li J, Fang Q, Liu Y, Zhang L (2014) A molecular dynamics investigation into the mechanisms of subsurface damage and material removal of monocrystalline copper subjected to nanoscale high speed grinding. *Appl Surf Sci* 303:331–343
28. Li J, Fang Q, Zhang L, Liu Y (2015) Subsurface damage mechanism of high speed grinding process in single crystal silicon revealed by atomistic simulations. *Appl Surf Sci* 324:464–474

**Publisher's note** Springer Nature remains neutral with regard to jurisdictional claims in published maps and institutional affiliations.